BRAF/MAPK and GSK3 signaling converges to control MITF nuclear export

Kao Chin Ngeow[a], Hans J. Friedrichsen[a], Linxin Li[a], Zhiqiang Zeng[b], Sarah Andrews[a], Laurent Volpon[c,d], Hannah Brunsdon[b], Georgina Berridge[a,e], Sarah Picaud[f], Roman Fischer[e], Richard Lisle[a], Stefan Knapp[f], Panagis Filippakopoulos[f], Helen Knowles[g], Eiríkur Steingrímsson[h], Katherine L. B. Borden[c,d], E. Elizabeth Patton[b], and Colin R. Goding[a,1]

[a]Ludwig Institute for Cancer Research, Nuffield Department of Medicine, University of Oxford, Headington, OX3 7DQ Oxford, United Kingdom; [b]Medical Research Council Human Genetics Unit & Edinburgh Cancer Research Centre, Medical Research Council Institute of Genetics and Molecular Medicine, University of Edinburgh, EH4 2XR Edinburgh, United Kingdom; [c]Institute for Research in Immunology and Cancer, Université de Montréal, Montréal, QC H3T 1J4, Canada; [d]Department of Pathology and Cell Biology, Université de Montréal, Montréal, QC H3T 1J4, Canada; [e]Discovery Proteomics Facility, Target Discovery Institute, Nuffield Department of Medicine, University of Oxford, Headington, OX3 7FZ Oxford, United Kingdom; [f]Structural Genomics Consortium, Nuffield Department of Medicine, University of Oxford, Headington, OX3 7DQ Oxford, United Kingdom; [g]Botnar Research Centre, Nuffield Department of Orthopaedics, Rheumatology and Musculoskeletal Sciences, University of Oxford, Headington, OX3 7HE Oxford, United Kingdom; and [h]Department of Biochemistry and Molecular Biology, Faculty of Medicine, University of Iceland, 101 Reykjavik, Iceland

Edited by Melanie H. Cobb, University of Texas Southwestern Medical Center, Dallas, TX, and approved August 1, 2018 (received for review June 21, 2018)

The close integration of the MAPK, PI3K, and WNT signaling pathways underpins much of development and is deregulated in cancer. In principle, combinatorial posttranslational modification of key lineage-specific transcription factors would be an effective means to integrate critical signaling events. Understanding how this might be achieved is central to deciphering the impact of microenvironmental cues in development and disease. The microphthalmia-associated transcription factor MITF plays a crucial role in the development of melanocytes, the retinal pigment epithelium, osteoclasts, and mast cells and acts as a lineage survival oncogene in melanoma. MITF coordinates survival, differentiation, cell-cycle progression, cell migration, metabolism, and lysosome biogenesis. However, how the activity of this key transcription factor is controlled remains poorly understood. Here, we show that GSK3, downstream from both the PI3K and Wnt pathways, and BRAF/MAPK signaling converges to control MITF nuclear export. Phosphorylation of the melanocyte MITF-M isoform in response to BRAF/MAPK signaling primes for phosphorylation by GSK3, a kinase inhibited by both PI3K and Wnt signaling. Dual phosphorylation, but not monophosphorylation, then promotes MITF nuclear export by activating a previously unrecognized hydrophobic export signal. Nonmelanocyte MITF isoforms exhibit poor regulation by MAPK signaling, but instead their export is controlled by mTOR. We uncover here an unanticipated mode of MITF regulation that integrates the output of key developmental and cancer-associated signaling pathways to gate MITF flux through the import–export cycle. The results have significant implications for our understanding of melanoma progression and stem cell renewal.

MITF | melanoma | MAPK | nuclear export | GSK3

The ability of transcription factors to respond to distinct signal transduction pathways and thereby implement gene expression programs characteristic of specific cell identities underpins development and is deregulated in disease. However, the output of discrete signaling modules should be integrated if complex microenvironmental cues are to be coordinated with cell behavior and the adoption of particular phenotypic states. This implies that those transcription factors with a key role in coordinating many aspects of cell biology may act as a nexus for multiple signaling pathways, integrating their output to fine-tune the expression of specific repertoires of target genes. Identifying how such master regulators of cell phenotype respond and coordinate multiple signaling inputs is key to deciphering the impact of signaling in development and disease.

The *MITF* gene encoding the microphthalmia-associated transcription factor not only determines cell identity in development but resides at the heart of melanocyte and melanoma biology where it coordinates a remarkably wide range of cell functions. MITF is a lineage survival oncogene (1) that cooperates with BRAF in melanoma initiation (2). It is required for melanoblast (3) and melanoma (4) survival and differentiation (5) but inhibits invasiveness (6) and tumor-initiation capacity (7). MITF has both a positive and negative role in cell division, promoting a differentiation-associated cell-cycle arrest (5) but also driving proliferation (6, 8). The positive and negative roles in melanoma and melanocyte proliferation have been explained by the so-called rheostat model for MITF function, in which its expression and activity increase as cells progress from invasiveness, through proliferation to differentiation (6, 9). Consistent with this, MITF is repressed by stresses that reprogram translation and drive invasion and drug and immunotherapy resistance (10). This model appears broadly to explain the correlations between MITF expression and invasive and proliferative phenotypes in melanoma. In addition, both low and high MITF have been associated with drug resistance (11–14), and siRNA-mediated depletion of MITF in melanoma triggers senescence (15). MITF has also been implicated

Significance

Signaling pathways ultimately exert their influence on cell behavior by regulating the activity of transcription factors that drive gene expression programs associated with specific cell phenotypes. How transcription factors integrate the outputs from multiple independent signaling events to coordinate cell behavior is a key issue. Here, we identify a regulated nuclear export signal in the lineage survival oncogene and cell fate-determining factor MITF. The regulated export signal integrates the outputs from the MAPK signaling pathway with those regulating GSK3 that play key roles in development and disease. The regulation of MITF nuclear export provides a means by which these key signaling pathways tune MITF activity that, in turn, controls cell identity in development and disease.

Author contributions: E.S., K.L.B.B., E.E.P., and C.R.G. designed research; K.C.N., H.J.F., L.L., Z.Z., S.A., L.V., H.B., G.B., and R.L. performed research; S.P., S.K., P.F., H.K., and E.S. contributed new reagents/analytic tools; K.C.N., H.J.F., L.L., Z.Z., S.A., L.V., G.B., R.F., and C.R.G. analyzed data; and K.C.N., H.J.F., L.L., S.A., L.V., R.F., and C.R.G. wrote the paper.

The authors declare no conflict of interest.

This article is a PNAS Direct Submission.

Data deposition: The proteomic data reported in this paper have been deposited in the ProteomeXchange Consortium database, proteomecentral.proteomexchange.org/cgi/GetDataset (identifier PXD010782).

[1]To whom correspondence should be addressed. Email: colin.goding@ludwig.ox.ac.uk.

This article contains supporting information online at www.pnas.org/lookup/suppl/doi:10.1073/pnas.1810498115/-/DCSupplemental.

Published online August 27, 2018.

in the biogenesis of both lysosomes (16, 17) and mitochondria (18, 19), thereby contributing to both autophagy and metabolism. Beyond melanocytes and melanoma, *MITF* is transcribed from alternative promoters generating isoforms with distinct first exons (20). These alternative isoforms promote differentiation of the retinal epithelium, osteoclasts, and mast cells (3) and recently have been implicated in the proliferation of pancreatic ductal adenocarcinoma (21).

Given the critical role of MITF in so many aspects of developmental and cancer biology, understanding whether and how it might integrate the output from the complex microenvironmental cues encountered by cells in development or in tumors is a key issue. Several posttranslational modifications of MITF have been identified to date, but the role of many is poorly understood. MITF is sumoylated at two sites, K182 and K316 (22–25), which is thought to promote differential target specificity. Importantly the MITF E318K mutation that prevents sumoylation on K316 predisposes to melanoma (24, 25), confirming the prooncogenic role of MITF. In addition to sumoylation, MITF is modified by several kinases. These include the mitogen-activated protein kinase (MAPK) ERK2 and RSK, with ERK-mediated phosphorylation on S73 reported to mediate increased binding to the p300 and CBP transcription cofactors (26), as well as ubiquitin-mediated degradation (27, 28). In osteoclasts, the stress-activated kinase p38 phosphorylates MITF on S307 to facilitate activation of gene expression (29) whereas phosphorylation of nonmelanocyte isoforms by TAK1 (30) or mTOR (31) mediates cytoplasmic retention via binding to a 14-3-3 protein. Whether p38, TAK1, and mTOR are MITF kinases in melanocytes/melanoma is unknown. GSK3, which is inhibited by both PI3K and Wnt signaling, has been reported to modify S298 to influence DNA binding (32), and more recently three C-terminal GSK3 sites have been implicated in controlling MITF protein stability (17). Whether and how other signals control MITF activity through posttranslational modification are unknown.

Here, we reveal that critical developmental signaling pathways already known to promote tumor initiation and senescence bypass in melanoma converge to control an ERK- and GSK3-regulated MITF nuclear export signal that regulates flux through the nuclear import–export cycle.

Results

In different tissues and cell types, MITF expression is controlled by distinct promoters, leading to the inclusion of different exons at the N terminus of the protein (20). In neural crest-derived melanocytes and melanoma, the MITF-M isoform predominates and is referred to here as MITF. Although many groups have focused on how changing MITF levels affect its function, the activity of MITF will also be influenced by its posttranslational modifications. However, despite several posttranslational modifications on MITF being identified (Fig. 1*A*), few have been assigned a clear regulatory function. Posttranslational modifications can potentially control transcription factor levels, interaction with cofactors, intramolecular conformation, DNA-binding affinity, or intracellular localization. To identify additional kinases that might affect MITF expression or subcellular localization, we undertook a phenotypic screen of SKmel28 human melanoma cells using a 367 compound small molecule kinase inhibitor library (33). Cells were treated with 2.5 μM of each compound and examined 6 h later using an anti-MITF antibody for immunofluorescence. The ratio of nuclear to cytoplasmic staining and the mean intensity of nuclear MITF were normalized relative to a corresponding DMSO-treated internal control. The preliminary results indicated that compounds targeting GSK3 (*SI Appendix*, Fig. S1*A*) promoted increased MITF nuclear accumulation at the expense of weak cytoplasmic staining that was reproducibly observed using different MITF antibodies. As an example, BIO, a selective, ATP-competitive inhibitor of GSK3 (34) increased MITF nuclear localization (Fig. 1*B*). β-catenin, which is degraded in response to GSK3-mediated phosphorylation, was used as a control. Similar results were obtained using SB-675259-M, a chemically distinct GSK3 inhibitor (*SI Appendix*, Fig. S1*B*). GSK3 is important as it is inhibited by PI3K signaling that is frequently activated in melanoma either through PTEN loss or via activating mutations in the PI3K catalytic subunit (35). In melanoma, PI3K signaling inhibits GSK3 activity and promotes resistance to anti-BRAF inhibitor therapies (36) and senescence bypass (37). GSK3 is also inhibited by WNT signaling that stabilizes β-catenin that can also promote senescence bypass in melanoma (38). Consistent with GSK3 targeting MITF, both the GSK3 inhibitor BIO or the structurally distinct GSK3 inhibitor SB-675259-M caused MITF to migrate at an intermediate position between the known hypophosphorylated lower form and the upper band that is known to be phosphorylated on S73 by ERK (39) when analyzed by SDS/PAGE and Western blotting (Fig. 1*C*).

One interpretation of these data is that phosphorylation by ERK on S73 promotes phosphorylation by GSK3 on another residue. As such, mutation of S73 would prevent phosphorylation by both kinases, but GSK3 inhibition would not affect phosphorylation by ERK. This model is attractive since GSK3 frequently requires a priming phosphorylation site; the consensus recognition motif for GSK3 is S-X-X-X-pS, with the first serine being phosphorylated by GSK3 after a priming phosphorylation on the serine at the +4 position (40). Examination of the MITF amino acid sequence in the vicinity of S73 revealed a potential GSK3 phosphorylation site at S69 that was evolutionarily conserved from zebrafish to humans (Fig. 1*D*). Moreover, a large-scale phosphoproteome analysis previously identified both S69 and S73 as being phosphorylated (41) although the nature of the relevant kinases and implications of phosphorylation were not examined. In this respect, the spacing between the ERK phosphorylation site at S73 and the GSK3 site at S69 matched the consensus and implied that ERK would act as the priming kinase.

This was confirmed using an in vitro kinase assay on a series of WT and mutated MITF peptides spanning S69 and S73 (Fig. 1*E*). Only peptide 6 containing an intact S69 as well as p-S73 was phosphorylated by purified GSK3β. A peptide (peptide 7) containing a substitution of S73 by a glutamic acid, frequently used to mimic phosphorylation, was not phosphorylated by GSK3β, highlighting the specificity of the S73 phosphorylation event in priming for GSK3β.

The results obtained using the peptide kinase assay were confirmed using a quantitative Mass Spec (MS) approach, in which the bacterially expressed and purified N-terminal domain of MITF (*SI Appendix*, Fig. S2*A*) was subject to phosphorylation in vitro using ERK and GSK3β alone or together (*SI Appendix*, Fig. S2 *B–E*). Quantification (*SI Appendix*, Fig. S2*F*) revealed that, while ERK phosphorylated S73 but not S69, the modification of S69 by GSK3β was inefficient unless S73 was phosphorylated.

Western blotting of extracts from cells expressing WT and mutant MITF further substantiated our conclusion that phosphorylation of S73 primes for GSK3-mediated phosphorylation at S69. Mutation of S69 led to MITF adopting an intermediate mobility (Fig. 1*F*), similar to that observed using GSK3 inhibitors (Fig. 1*C*), whereas mutation of S73, as predicted, led to a complete shift to the lower position. No effect on MITF mobility was detected after mutation of S298 that has previously been reported as a GSK3 target (32). Both the upper and lower bands were shifted down if the three C-terminal GSK3 sites identified by Ploper et al. (17) were mutated although the ratio between the upper and lower bands was maintained and no substantial effect on protein levels was observed. Phosphatase treatment of extracts from 501mel cells transfected with FLAG-tagged WT and mutant MITF followed by Western blotting led to increased mobility of MITF to a position below that of the S73A mutant (Fig. 1*G*). This result is consistent with MITF being phosphorylated on multiple residues in addition to S73 and S69, including the C-terminal GSK3 phosphorylation sites. Note that the charge on the glutamic acid substitution mutants results in a small reduction in protein mobility.

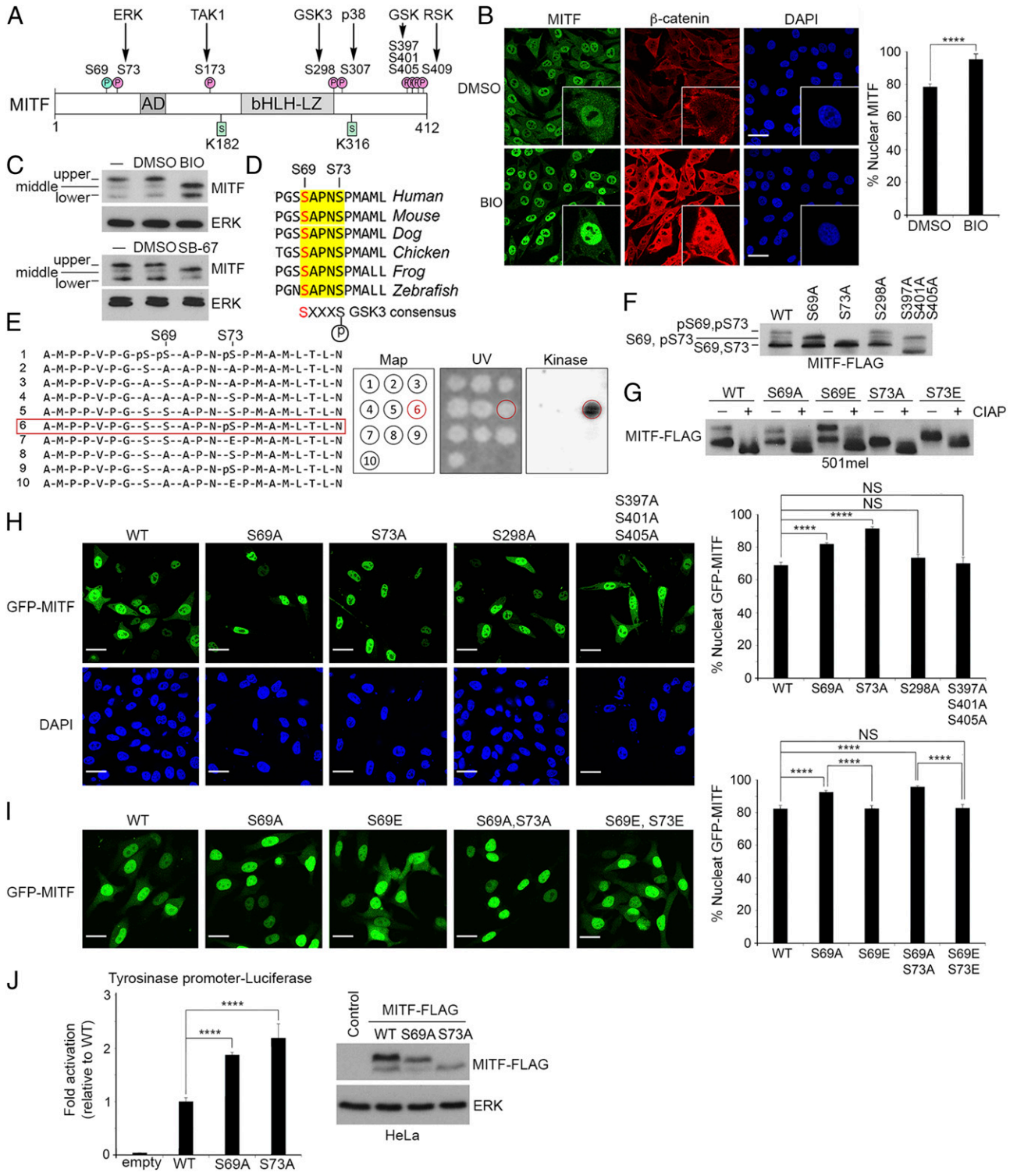

Fig. 1. GSK3 phosphorylates MITF S69 to control MITF subcellular localization. (*A*) MITF posttranslational modifications. (*B*) Immunofluorescence of SKmel28 cells following treatment with 1 μM BIO or DMSO for 18 h. Cells were stained with DAPI (blue) and antibodies against MITF (green) or β-catenin (red). Quantification (*Right*). n > 70 per condition. Error bars represent SEM. Two-tailed *t* test: ****$P < 0.0001$. (*C*) Western blot of SKmel28 cells following treatment with 1 μM BIO, 1 μM of SB-675259-M, or DMSO as in *A*. (*D*) Amino acid sequence alignment of MITF. In the GSK3 consensus, X = any amino acid. (*E*, *Left*) Twenty-one residue peptides corresponding to MITF amino acids 61 to 81 used for the SPOT kinase assay immobilized on a cellulose support membrane. (*E*, *Right*) SPOT kinase assay using purified GSK3β. A map showing the identity of the 10 tested peptides (*Left*) corresponding to peptide spots on the membrane imaged in UV light (*Middle*), and the kinase assay (*Right*). (*F*) Western blot of 501mel cells ectopically expressing indicated MITF-FLAG WT and mutants. (*G*) Western blot of extracts from 501mel cells ectopically expressing indicated MITF-FLAG WT and mutants treated or not with calf intestinal phosphatase (CIAP). (*H* and *I*) Fluorescence images of 501mel cells ectopically expressing GFP-MITF WT and indicated mutants (green). (Scale bars: 10 μm.) Quantification (*Right*). $n > 40$ per condition. Error bars represent SEM. Two-tailed *t* test (*Upper*) and one-way ANOVA with post hoc Tukey test: ****$P <$ 0.0001, NS, not significant, $P > 0.05$. (*J*) Luciferase assay with MITF-FLAG WT and mutants and a TYR promoter-Luc reporter cotransfected into HeLa cells. Error bars represent SEM. Two-tailed *t* test: ****$P < 0.0001$. Western blot shows relative expression of WT and mutant MITF-FLAG proteins.

Using an MITF–GFP fusion protein expressed in MITF-negative HeLa cells confirmed that the cytoplasmic fluorescence detected using the WT protein was abolished by either the S69A or S73A mutations whereas mutating either S298 or the C-terminal GSK3 sites had no effect on MITF localization (Fig. 1*H*). Moreover, introduction of phosphomimetic glutamic acid substitutions at S69 or at both S69 and S73 gave a similar pattern of cytoplasmic MITF localization as the WT (Fig. 1*I*) while the S69A and S69A, S73A mutants were significantly more nuclear. Note that the S69E mutant was significantly more cytoplasmic than the S69A mutant, suggesting that S69 may control subcellular localization. Moreover, the increased nuclear localization of the S69A and S73A mutants was reflected in their increased capacity to activate a Tyrosinase-promoter-luciferase reporter (Fig. 1*J*).

Cytoplasmic Accumulation of MITF in Response to BRAF/MAPK Signaling. To examine the impact of regulating MAPK signaling on MITF subcellular localization, we treated 501mel melanoma cells with 12-*O*-tetradecanoylphorbol-13-acetate (TPA). TPA efficiently promoted ERK phosphorylation and a mobility shift in MITF consistent with increased phosphorylation on S73, with both being blocked by the MEK inhibitor U0126 (Fig. 2*A*). As anticipated, given the role of S73 phosphorylation in priming GSK3-mediated modification of S69, TPA increased nuclear localization of activated ERK and the proportion of cytoplasmic MITF, an effect blocked using U0126 (Fig. 2*B*). MITF cytoplasmic accumulation in response to TPA was prevented using the GSK3 inhibitor BIO (Fig. 2*C*), as well as by the S73A mutation, and was reduced using the S69A mutant (Fig. 2*D*), indicating that phosphorylation on S73 in the absence of S69 phosphorylation can make a contribution to MITF's subcellular localization independently of its ability to promote S69 phosphorylation. Similar results were obtained in HeLa cells where induction of doxycycline-inducible $BRAF^{V600E}$ promoted cytoplasmic localization of WT MITF-GFP (Fig. 2*E*), which was blocked using U0126, but did not trigger cytoplasmic accumulation of the S73A mutant.

MITF Contains a BRAF/MAPK-Regulated Nuclear Export Signal. Although TPA induced MITF to be completely phosphorylated at S69 and S73 (Fig. 2*A*), TPA did not induce all endogenous MITF to be localized to the cytoplasm (Fig. 2*B*). The balance between cytoplasmic and nuclear localization will be influenced by several factors, including the relative rate of nuclear import and export. MITF's nuclear import is mediated by a constitutive nuclear localization signal in the basic region of the bHLH-LZ domain (42). Whether MITF is subject to active nuclear export is not known. Preliminary evidence indicated that the N-terminal region of MITF (residues 1 to 180) could relocalize to the cytoplasm in response to TPA treatment (*SI Appendix*, Fig. S3*A*). Moreover, a series of N-terminal deletion mutants revealed that TPA was able to promote cytoplasmic localization of MITF lacking the N-terminal 60 amino acids but was unable to do so if an additional 40 amino acids were removed (*SI Appendix*, Fig. S3*B*). Thus, residues 60 to 100, which contain the S69 and S73 regulatory phosphorylation sites, were required for TPA-induced cytoplasmic localization. Examining the amino acid sequence in the vicinity of S73, the key regulator of MITF cytoplasmic accumulation, revealed a hydrophobic patch (MxMLxL) that resembled a classical nuclear export signal (NES) (43)

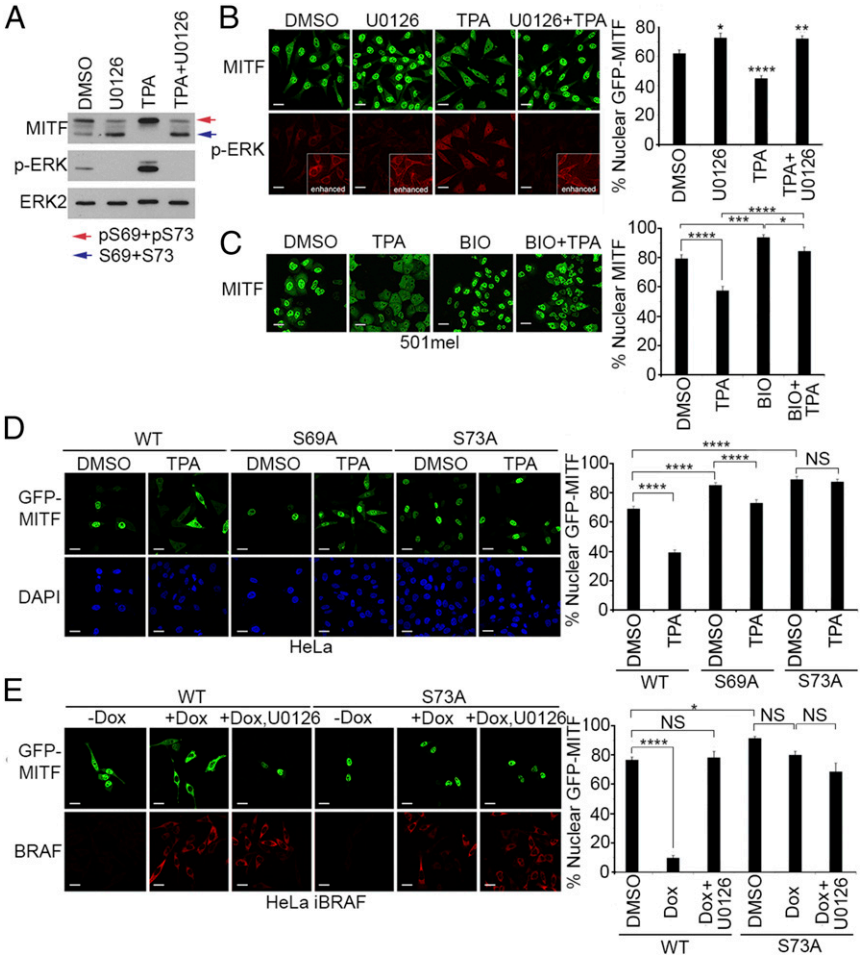

Fig. 2. BRAF/MAPK signaling redirects MITF to the cytoplasm. (*A*) Western blot or (*B*) immunofluorescence of 501mel cells following 200 nM TPA treatment (1 h) in the presence or absence of 10 μM U0126 (3 h). After fixation and permeabilization, the cells were stained with the nucleic acid stain DAPI (blue) and antibodies against MITF (green) or phospho-ERK (red). n >100 for each condition. (*C*) Immunofluorescence of 501mel cells treated with 200 nM TPA (1 h) and/or 1 μM BIO. $n > 40$ cells per condition. (*D*) Fluorescence assay of 501mel cells ectopically expressing WT or mutant MITF-GFP and treated with 200 nM TPA for 1 h as indicated. $n > 49$ for each condition. (*E*) Immunofluorescence of Flip-in HeLa cells engineered to express doxycycline-inducible $BRAF^{V600E}$-FLAG ectopically expressing GFP-MITF WT or the S73A mutant (green). Twenty-four hours posttransfection, cells were treated with 2 ng/mL doxycycline for 24 h and treated as indicated with 10 μM U0126 for 3 h. Anti-FLAG-BRAF (red). $n > 10$ cells per condition. Quantification by two-tailed *t* test or one-way ANOVA with post hoc Tukey test (*E*):*$P < 0.05$; **$P < 0.01$; ***$P < 0.001$; ****$P < 0.0001$; NS, not significant, $P > 0.05$; error bars represent SEM.

(Fig. 3*A*). We confirmed that MITF is subject to active export from the nucleus using leptomycin B (LMB), an inhibitor of chromosome maintenance 1 (CRM1)-mediated export (44), which increased nuclear localization of MITF (Fig. 3*B*) and prevented cytoplasmic accumulation of MITF-GFP in response to TPA treatment (Fig. 3*C*). Consistent with these observations, MITF was able to directly interact with CRM1 in a RAN-GTP–dependent fashion in vitro using bacterially expressed and purified proteins (Fig. 3*D*), consistent with results from a previous deep proteomic assay for CRM1 interactions (45).

To determine whether this region of MITF contains a functional NES, we used a GFP-based fluorescent NES reporter vector. Since the final size of any GFP fusion protein in the reporter needed to be greater than 40 kDa to prevent passive diffusion between the cytoplasm and nucleus (46), GST was fused in frame with GFP. The parental GFP-GST reporter was largely cytoplasmic (*SI Appendix*, Fig. S4*A*). The addition of a nuclear localization signal (NLS), PKKKRKV, from the simian virus 40 (SV40) T-antigen (47), led to the reporter being expressed in the nucleus. Further addition of a classical NES, LALKLAGLDI, from the cAMP-dependent protein kinase inhibitor (PKI) (48) served as a positive control for nuclear export, relocalizing the NLS-containing reporter protein to the cytoplasm. TPA had no effect on the localization of any of these proteins. Replacement of the PKI NES with MITF amino acids 60 to 99 led to the reporter being distributed between the nucleus and cytoplasm (Fig. 3*E*), but addition of TPA promoted cytoplasmic localization. Consistent with our previous observations, the S73A mutant was unresponsive to TPA and was localized primarily to the nucleus whereas the S69A mutant largely abrogated the increased cytoplasmic localization triggered by TPA. Importantly, the MEK inhibitor U0126 significantly reduced the cytoplasmic localization induced by TPA while the reporter was almost completely localized in the nucleus in the presence of LMB, irrespective of the presence or absence of TPA (Fig. 3*F*). Collectively, these data are consistent with MITF containing a MAPK and GSK3 coregulated NES.

To characterize better the requirements for MITF nuclear export, we used the same GFP-NLS-GST reporter to analyze the effect of mutations in the putative hydrophobic NES. Single alanine substitutions in M75, L78, and L80 all abrogated the relocalization to the cytoplasm in response to TPA (*SI Appendix*, Fig. S4*B*). By contrast, mutation of M77 had no effect. The role of M75, L78, and L80 in nuclear export was confirmed in the context of full-length MITF where the relocalization of the WT protein to the cytoplasm in response to TPA was prevented by alanine substitution in any of these three residues (*SI Appendix*, Fig. S4*C*). Importantly, mutation of L75, L78, or L80 did not affect the ERK-mediated mobility shift in MITF in response to TPA arising via phosphorylation of S73 (*SI Appendix*, Fig. S4*D*).

Regulation of Nonmelanocyte Isoforms. The results so far suggest that phosphorylation of MITF on S73 by ERK downstream from BRAF triggers GSK3-mediated phosphorylation of S69 and, consequently, NES-mediated MITF nuclear export. In melanoma cells, activation of this pathway, by induction of MAPK activity in response to TPA or BRAF for example, leads to an increased proportion of MITF relocalizing to the cytoplasm. However, under standard growth conditions, only 10 to 20% of endogenous MITF is cytoplasmic, most likely reflecting the fact

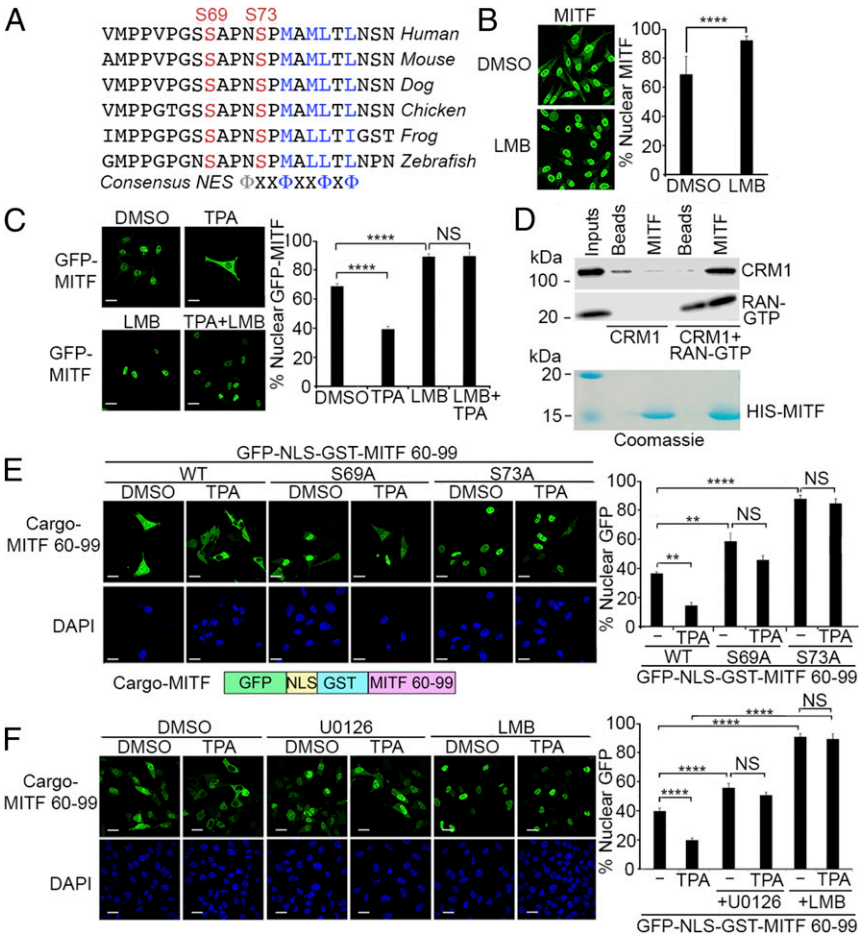

Fig. 3. MITF has a nuclear export signal. (*A*) Alignment of MITF sequences in the vicinity of S69 and S73 from different species. Hydrophobic residues highlighted in blue indicate the putative NES. (*B*) Immunofluorescence of endogenous MITF in 501mel cells treated with 20 nM LMB for 3 h as indicated. $n > 80$ cells per condition. (*C*) Fluorescence images of 501mel cells ectopically expressing WT GFP-MITF (green) treated with 200 nM TPA for 1 h and/or 20 nM LMB for 3 h. $n > 49$ per condition. (*D*) CRM1 pull-down assay using bacterially expressed HIS-Tagged MITF (1–105) bound to Ni-NTA beads. All proteins were bacterially expressed and purified, and, after pull-down, CRM1 and RAN were detected by Western blotting using specific antibodies. Purified MITF was visualized by Coomassie staining (*Lower*). (*E* and *F*) Fluorescence assay of 501mel cells transfected with indicated GFP reporters. $n > 43$ per condition. Quantification by two-tailed *t* test: $^{**}P < 0.01$; $^{****}P < 0.0001$; NS, not significant, $P > 0.05$; error bars represent SEM.

that nuclear import is efficient and that the melanocyte-specific isoform of MITF, MITF-M, is not retained in the cytoplasm. By contrast, other isoforms of MITF bearing different first exons arising from differential promoter usage (20) can localize to the cytoplasm more completely owing to cytoplasmic retention following phosphorylation of S173 by TAK1 in osteoclasts (30), or by phosphorylation by mTORC1 and the interaction with the RAG GTPases at the surface of the lysosome (31). We therefore examined the impact of inhibiting nuclear export of the MITF-A and MITF-D isoforms. In both cases, transfection of HeLa cells with MITF-A or MITF–D expression vectors led to a largely cytoplasmic localization (Fig. 4*A* and *SI Appendix*, Fig. S5*A*). Cytoplasmic retention of the nonmelanocyte isoform MITF-A was prevented by mutation of conserved residues Q62 and L63 within exon B1b (*SI Appendix*, Fig. S5*B*) that is required for interaction with the RAG GTPases (31), and by Torin 1 (*SI Appendix*, Fig. S4*A*), an inhibitor of mTOR that phosphorylates on an MITF-M S173-equivalent residue to promote cytoplasmic retention via phosphorylation-mediated 14-3-3 binding.

However, in both MITF-A and MITF-D, nuclear export is also important since treatment with either LMB or the GSK3 inhibitor BIO led to increased accumulation of MITF-A or MITF-D within the nucleus (Fig. 4*A* and *SI Appendix*, Fig. S5*A*). Moreover, introducing the MITF-M L80A equivalent into the MITF-A and MITF-D isoforms also substantially increased nuclear retention of each isoform. Inhibition of MEK, using U0126 to reduce MAPK activity, also increased MITF-A and -D nuclear localization to a similar extent as BIO, but less than Torin 1, indicating that ERK-mediated phosphorylation of MITF makes a previously unrecognized contribution to the subcellular localization of nonmelanocyte isoforms.

These observations were confirmed by examining endogenous MITF in both retinal pigment epithelia (RPE) ARPE19 cells, which express multiple nonmelanocyte MITF isoforms (20), and osteoclasts, which express both the MITF-A and -D isoforms (49). LMB promoted dramatically increased nuclear localization of MITF in the *ARPE19* RPE cell line (Fig. 4*B*), and, in osteoclasts, MITF nuclear accumulation was also increased in response to BIO, U0126, Torin 1, and LMB (*SI Appendix*, Fig. S5*C*). The results obtained using LMB reveal that regulated nuclear export plays a key role in controlling the nuclear availability of endogenous MITF in these cells. These data indicate that the nuclear export signal is highly active in different MITF isoforms. The reason the endogenous MITF-M isoform does not more efficiently accumulate in the cytoplasm under steady-state conditions is most likely the absence of alternative exon 1B1b since mutation of the RAG GTPase interaction motif generated predominantly nuclear MITF-A (*SI Appendix*, Fig. S5*B*).

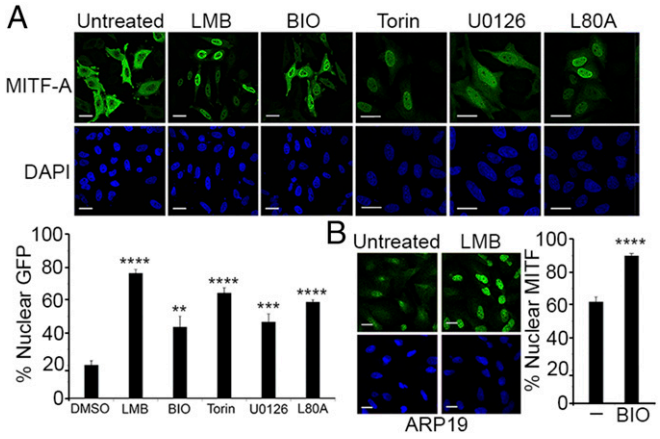

Fig. 4. Regulated nuclear export of MITF-A isoforms. (*A*) Immunofluorescence using anti-MITF antibody of HeLa cells transfected with expression vectors for MITF-A isoform treated with indicated drugs (20 nM LMB; 10 μM U0126; 200 nM Torin 1; 1 μM BIO) or expressing the L80A mutant. $n > 20$ cells per condition. (*B*) Immunofluorescence using anti-MITF of ARP19 (RPE) cells with or without 20 nM LMB. $n > 20$ cells per condition. (Scale bars: 10 μm.) Quantifications by two-tailed t test: $^{**}P < 0.01$; $^{***}P < 0.001$; $^{****}P < 0.0001$. Error bars represent SEM.

MITF S69 Is Critical for Melanocyte Development. To investigate the possibility that S69 was important in melanocyte development, we mutated the equivalent of the S69 residue in zebrafish Mitfa to alanine, which prevents phosphorylation, or glutamic acid, which can mimic constitutive phosphorylation. We then injected plasmids encoding these mutants under the control of the fish Mitfa promoter into *mitfa*-null *nacre* zebrafish embryos and determined if the mutants could rescue melanophore development in these embryos. The results (Fig. 5) revealed that the S69A mutant could rescue melanophore development (number of embryos = 29, mean number of melanophores per embryo = 6.1), as did WT Mitfa ($n = 11$, mean = 9.9). Although there were fewer melanophores per embryo with the S69A mutant compared with the WT, there were no significant differences between the WT and mutant variants as determined by one-way ANOVA test [95% CI: (−0.876, 8.418)]. On the other hand, the phosphomimetic S69E mutant, that exhibits significantly increased cytoplasmic localization compared with S69A (Fig. 1*I*), failed to rescue melanophore development in all injected embryos ($n = 26$, mean = 0). WT and mutant Mitfa were similarly expressed in *mitfa*-null zebrafish embryos (*SI Appendix*, Fig. S6). However, while there is a clear difference in the ability of the S69A and S69E mutants to complement the lack of MITF in zebrafish consistent with the phosphorylation status of S69 in MITF being critical for melanocyte development, the absence of antibodies able to recognize MITF or phospho-S69 in fish means that the role of S69 phosphorylation in MITF nuclear export in this model requires further validation.

Discussion

Many nuclear export signals have been characterized (43), and some, like the yeast transcription factor Pho4 (50) or cyclinD1 (51), are regulated by phosphorylation. However, the NES in MITF is highly unusual in the sense that it acts as a nexus for key developmental signaling pathways implicated in melanoma initiation and progression (Fig. 6). In the melanocyte-specific MITF isoform, MITF-M, phosphorylation of S73 by ERK downstream from BRAF and NRAS primes for phosphorylation of S69 by GSK3.

Under standard culture conditions, GSK3 is active, and, consequently, it is the priming activity of ERK that dictates whether the MITF NES operates. Despite the melanoma cells used here having a $BRAF^{V600E}$ mutation, ERK activity is not maximal and can be stimulated by TPA, leading to increased cytoplasmic localization of MITF-M. However, GSK3 activity can be suppressed by PI3K signaling that is frequently activated in melanoma: for example, by loss of PTEN. Since both ERK- and GSK3-mediated phosphorylation events are necessary for efficient export to occur, the MITF export signal potentially provides a route to integrate MAPK and PI3K signaling with regulation of MITF's target genes implicated in both proliferation and differentiation. Mechanistically, we view it likely that the hydrophobic MITF nuclear export signal may be occluded by an intramolecular interaction and that the phosphorylation events alter the conformation to unmask the export signal. In this scenario, a single phosphorylation event on S73 may contribute, but the dual phosphorylation on S73 and S69 will be more efficient, as in fact we observed.

Although the level of endogenous MITF-M observed in the cytoplasm is relatively low in melanoma cells in culture, the steady-state ratio of nuclear to cytoplasmic MITF is likely to be less important than flux through the import–export cycle. For any transcription factor, nuclear localization is necessary for it to find its target genes. The probability of its being able to do so will

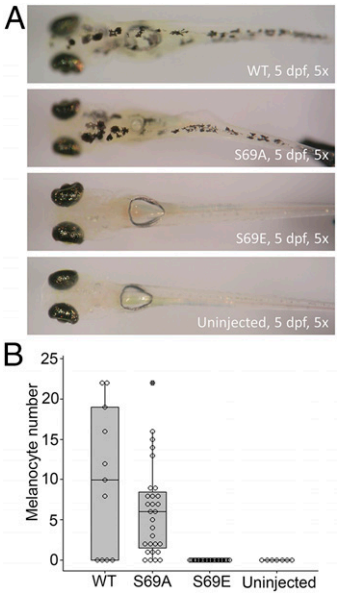

Fig. 5. MITF S69 is required for melanocyte development. (*A*) Representative images of *mitfa*-null *nacre* embryos injected with plasmids encoding Mitfa WT or indicated mutants taken 5 d postfertilization (dpf). (*B*) Quantification of the number of rescued melanocytes per embryo. Mitfa WT (number of embryos n = 11, mean melanocytes per embryo = 9.9); S69A mutant (number of embryos = 29, mean number of melanocytes per embryo = 6.1); S69E number of embryos = 25, mean = 0). For WT vs. S69A: no significant difference by one-way ANOVA test [95% CI: (−0.876, 8.418)] (experimental replicates n = 3).

depend on its residence time in the nucleus. Activation of the MITF NES will lead to decreased nuclear residence time and is therefore likely to diminish the ability of MITF to bind and regulate its targets. As such, even a 10% increase in the cytoplasmic localization may in reality reflect a far greater effect on productive MITF DNA-binding and gene regulation. Moreover, phosphorylation of S73 by ERK has been reported to promote proteasome-mediated degradation of MITF (27, 28) although we have not detected any increased expression of an S73A mutant versus the WT protein. Nevertheless, the role of S73 phosphorylation in stimulating export raises the possibility that export may enhance cytoplasmic MITF turnover, and, consequently, the levels of steady state cytoplasmic MITF may be underestimated.

In contrast to MITF-M, where the majority of the protein is nuclear under standard culture conditions, the nonmelanocyte MITF isoforms that are critically required for development of mast cells, osteoclasts, and the RPE are predominantly cytoplasmic. Since inhibition of the NES using LMB promotes localization of MITF-A and -D to the nucleus, it seems that the nonmelanocyte isoforms are constantly passing through the import–export cycle, with their predominantly cytoplasmic localization arising as a result of cytoplasmic retention. This occurs because the nonmelanocyte MITF isoforms, but not MITF-M, contain residues within their N-terminal region that mediate binding to RAG GTPases at the lysosomal surface where they can be phosphorylated by the nutrient sensing mTORC1 complex (31). Phosphorylation of nonmelanocyte isoforms by mTORC1 at S173 (using MITF-M numbering) will lead to cytoplasmic retention by promoting interaction with a 14-3-3 protein (30). Consequently, inhibition of mTOR using Torin 1 or mutation of the RAG-interacting region leads to their nuclear accumulation. Since inactivation of mTORC1 via nutrient limitation will lead to nuclear accumulation of the nonmelanocyte isoforms (31), the NES identified here will play a key role in restoring cytoplasmic MITF localization when nutrient levels are restored. However, the biological reason why the melanocyte-specific MITF-M isoform is not regulated by mTOR remains unclear. One possibility is that, during melanoblast migration, mTOR-mediated MITF export and cytoplasmic retention would be incompatible with regulation of MITF-driven melanoblast proliferation, and, consequently, MITF-M needs to be uniquely perceptive to MAPK signaling.

Although, for technical reasons, we have been unable to measure MITF phosphorylation in the fish model, an S69E substitution in Mitfa prevents melanocyte development whereas an S69A mutation complements MITF loss efficiently. These observations suggest that the phosphorylation status of S69 may be important during melanocyte development. We also envisage there may be two additional scenarios where a regulated MITF-M export signal may be important.

First, activation of BRAF or NRAS by mutation in primary melanocytes in vivo would trigger an instantaneous increase in MAPK signaling and consequently decrease MITF nuclear localization by promoting export. Since, in primary melanocytes, activating mutations in *BRAF* or *NRAS* trigger senescence, it is possible that the downstream activation of MAPK signaling would increase MITF export, as we observed following induction of $BRAF^{V600E}$ expression, thereby preventing MITF driving proliferation. Since depletion of MITF in cells bearing activated BRAF triggers senescence (15), these observations are consistent with a model in which an active MITF NES might pose a barrier to BRAF-mediated melanoma initiation in vivo. Additional mutations in signaling pathways leading to inactivation of GSK3 would prevent MITF export and, consequently, complement BRAF activation by enabling MITF to remain nuclear to stimulate proliferation. Consistent with this scenario, PI3K (37) and WNT signaling (38) both inhibit GSK3 and are implicated in senescence bypass in melanoma (52–54). We also note that GSK3 can be inhibited by phosphorylation by p90 RSK lying downstream from ERK and BRAF (55). Although we have not examined the impact of BRAF activation on GSK3 activity, the possibility that BRAF activation can lead to inhibition of GSK3 suggests that the MITF export signal may be also be modulated by the kinetics of RSK activation in response to different upstream signals.

Secondly, while the MITF-M NES might provide a mechanism to protect against cancer initiation, its primary purpose will be to regulate MITF activity under physiological conditions. WNT signaling increases MITF-M protein stability by preventing phosphorylation of the C-terminal GSK3 sites (17) and also increases MITF-M mRNA expression via β-catenin–mediated activation of the MITF-M promoter (56), an event that commits cells to a melanocyte lineage fate to generate melanoblasts (57). Our results suggest that inhibition of GSK3 by WNT might also promote MITF activity by preventing MITF nuclear export. Moreover, WNT-mediated activation of melanocyte stem cells in the hair follicle bulge (58) should drive proliferation by both increasing MITF expression and preventing MITF export. We also note that a point source of WNT can promote cell division

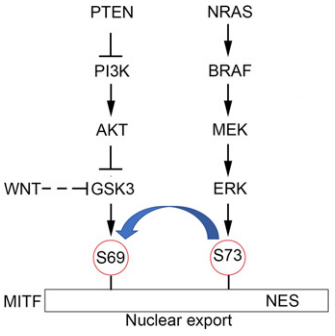

Fig. 6. Model illustrating potential regulation of MITF nuclear export.

in the plane of the WNT signal (59), giving rise to two daughter cells, with either high WNT signaling and consequently low GSK3 activity close to the source, or low WNT signaling and high GSK3 in the daughter cell furthest from the source. In principle, this would create two daughter cells with differential activity of the MITF export signal. If point source WNT signaling occurs in the melanocyte stem cell niche, the regulated export signal has the potential to decrease MITF activity in the distal daughter cell, an event that would facilitate stem cell renewal. While this model is speculative, it does provide a framework for studies that would investigate the potential role of the MITF export signal in stem cell renewal.

While we confirmed that MITF is phosphorylated by GSK3 at its C terminus as described previously (17), we saw no effect of mutating the reported (32) S298 GSK3 phosphorylation site on MITF subcellular localization or mobility by SDS/PAGE. Moreover, this site is not localized near any putative priming phosphorylation site that is usually required for GSK3-mediated phosphorylation. Given that S298 lies at the end of the MITF leucine zipper and is not able to mediate DNA contact (60), it is difficult to understand mechanistically how it can affect DNA recognition as reported (32). Moreover, in a separate study, Grill et al. (61) showed that the S298A mutation did not have any significant effect on MITF's ability to bind DNA or transactivate the *TYR* promoter, as well as other downstream targets such as the *TYRP1* and *DCT* promoters. We therefore feel it unlikely that S298 represents a bona fide GSK3 phosphorylation site.

Materials and Methods

Cell Culture, Transfection, and Chemicals. Established human melanoma cell lines, including 501mel and SK-MEL-28 (available from the American Type Culture Collection), were grown in Roswell Park Memorial Institute (RPMI) 1640 media (Invitrogen), supplemented with 10% FBS (PAA Laboratories) and 50 units/mL penicillin, 50 μg/mL streptomycin (Invitrogen). Cell lines of nonmelanocytic origin, including HeLa and Phoenix-AMPHO, were grown in Dulbecco's modified Eagle's medium (DMEM), supplemented with 10% FBS and 50 units/mL penicillin, 50 μg/mL streptomycin. All cells were grown in humidified incubators at 37 °C with 10% CO_2. Cell lines used were authenticated by EUROFINS using short tandem repeat (STR) profiling and mycoplasma screening conducted monthly.

Osteoclasts were isolated from peripheral blood mononuclear cells isolated from leukocyte cones (National Blood Service) by density gradient centrifugation. $CD14^+$ monocytes were positively selected using magnetic beads (Miltenyi) and seeded onto glass coverslips in α-MEM culture media (without ribonucleosides/deoxyribonucleosides; Lonza) containing 10% FBS, L-glutamine (2 mM), penicillin (50 IU/mL), and streptomycin sulfate (50 μg/mL). Cultures were supplemented with macrophage colony-stimulating factor (M-CSF) (25 ng/mL; R&D Systems) and receptor activator of nuclear factor kappa B ligand (RANKL) (35 ng/mL; produced in house) every 3 to 4 d. Mature osteoclasts, considered as multinucleated cells containing ≥3 nuclei, formed by day 9.

Transient transfection of DNA was carried out using FuGENE 6 (Promega) according to the manufacturer's instructions.

HeLa Flp-In T-REx cells were maintained as per WT HeLa cells, but with a further supplement of 4 μg/mL blasticidin to maintain TetR expression and 50 μg/mL zeocin to ensure that the flippase (Flp) recombination target (FRT) sites were retained. HeLa Flp-In T-REx cells were cotransfected with the pcDNA5/FRT/TO plasmid expressing the $BRAF^{V600E}$ under the control of a tetracycline-regulated CMV/$TetO_2$ promoter, and the pOG44 plasmid that expresses the Flp recombinase under a constitutive CMV promoter at a 3:1 ratio of pcDNA5/FRT/TO to pOG44. Transfected cells were selected with 200 μg/mL hygromycin and 4 μg/mL blasticidin. Stable polyclonals were observed after 2 wk of antibiotic selection.

Doxycycline, TPA, and LMB were obtained from Sigma-Aldrich, BIO from Merck, and U0126 and Torin 1 from Cell Signaling Technology.

Expression Vectors and Site-Directed Mutagenesis. MITF-FLAG or MITF-GFP and derivatives were made by cloning the MITF-M cDNA into p3xFLAG-CMV-14 (Sigma) or pEGFP-C1 (Clontech). The NES reporter was also constructed using pEGFP-C1. $BRAF^{V600E}$ cDNA was inserted into pcDNA5/FRT/TO (Invitrogen). Point mutations were introduced using the QuikChange Lightning Site-Directed Mutagenesis (SDM) Kit (Agilent) according to the manufacturer's instructions.

Western Blotting. Following SDS/PAGE, proteins were transferred to a Protran nitrocellulose membrane (Whatman) via electroblotting in transfer buffer (25 mM Tris, 192 mM glycine, 20% methanol) at 70 V for 90 min. The membrane was blocked with 5% skimmed milk in 0.1% Tween in PBS (PBST) for 1 h at room temperature, after which it was incubated with the primary antibody (typically diluted 1:2,000 in 5% milk in PBST) at 4 °C overnight with gentle agitation on a rocking platform. The membrane was then washed three times with PBST for 5 min each time and incubated with the corresponding horseradish peroxidase (HRP)-conjugated secondary antibody (Bio-Rad) (diluted 1:5,000 in 5% milk in PBST) for 1 h at room temperature, before another 3× 5-min wash in PBST. Finally, enhanced chemiluminescence (ECL) reagent (Amersham) was added, and the signal was detected with X-ray film (Fujifilm).

Antibodies. Antibodies used were as follows: rabbit anti–β-catenin (ab2365; Abcam), mouse anti-FLAG (monoclonal M2; Sigma), rabbit anti-ERK (C14; Santa Cruz), mouse anti-MITF (monoclonal AS9; in house), rabbit anti–phospho-ERK (Cell Signaling), rabbit anti–phospho-β-catenin (Cell Signaling), anti-CRM1 (Santa Cruz), and anti-RAN (BD Biosciences).

Immunofluorescence and Kinase Inhibitor Screen. Cells were grown to 80% confluence on glass coverslips (VWR) and fixed with 3.7% paraformaldehyde (PFA) (Sigma-Aldrich), dissolved in PBS and adjusted to pH 7.4, for 15 min. After 30 min blocking and permeabilization with 0.1% Triton-X and 1% BSA in PBS, cells were incubated with primary antibody (diluted 1:500 in 1% BSA in PBST) at 4 °C overnight with gentle agitation on a rocking platform. After washing three times with PBST for 5 min each time, the cells were incubated with the appropriate Alexa Fluor-conjugated secondary antibody (Invitrogen) (diluted 1:1,000 in 1% BSA in PBST) for 1 h, before another 3× 5-min wash in PBST. DNA was stained with 300 nM 4′,6-diamidino-2-phenylindole (DAPI) (Invitrogen) in PBS for 15 min, before a 3× 5-min wash in PBST. Coverslips were mounted on microscope glass slides (VWR) with Vectashield Mounting Medium (Vector Laboratories) before sealing with nail polish. Images were acquired using an LSM710 confocal microscope (Carl Zeiss).

For cells expressing fluorescent proteins, cells were stained with DAPI after PFA fixation. Blocking, permeabilization, and antibody staining steps were omitted unless detection of nonfluorescent proteins was required. The coverslips were then mounted and imaged as above.

For the small molecule library screen, ∼5,000 SKmel28 melanoma cells were seeded into each well of 96-well black CellCarrier plates (PerkinElmer) with optically clear plastic bottoms. Cells were grown to 80% confluence overnight, upon which they were treated for 6 h with 2.5 μM of each compound from the Glaxo Smith Kline (GSK) Published Kinase Inhibitor Set. Cells were then processed as described in the immunofluorescence protocol.

The quantification of (immuno)fluorescence images was performed using ImageJ. Nuclear masks were created by DAPI staining, and cytoplasmic masks by either Phalloidin or Cell Tracker Orange (Thermo Fisher). The percentage of nuclear MITF intensity was calculated by (MITF in nucleus)/(MITF in whole cell) × 100% on a per cell basis. Three independent experiments were performed for each quantification with a minimum of 40 cells (****$P < 0.0001$, ***$P < 0.001$, **$P < 0.01$, *$P < 0.05$, NS, nonsignificant).

SPOT Kinase Assay. Twenty-one-residue-long peptides corresponding to MITF residues 61 to 81, and incorporating various mutations and modifications, were immobilized on a cellulose support membrane. The membrane was then incubated with 100 ng of purified GSK3β kinase (New England Biolabs) and 5 μCi of [γ-^{32}P]-ATP at 30 °C for 30 min. After washing, incorporation of ^{32}P was detected by phosphorimager. The membrane was imaged in UV light to show the relative size of the peptide spots.

Bacterial Expression of MITF and in Vitro Phosphorylation. Recombinant 6× HIS-Tagged MITF (1–100) was expressed in *Escherichia coli* (Rosetta) by adding 0.1 mM IPTG and incubating overnight at 18 °C. After harvesting, cells were lysed in a buffer containing 6 M urea, 25 mM Hepes, pH 7.5, 0.5 M NaCl, 5% glycerol, 20 mM imidazole buffer, pH 7.5, using a French press homogenizer. After centrifugation of the lysate at 25,000 × *g* for 15 min, the supernatant was mixed with Ni-NTA agarose beads (QIAGEN), incubated at 4 °C while rotating for 1 h, and then placed in a gravity-flow column. Beads were then washed twice with wash buffer (6 M urea, 25 mM Hepes, pH 7.5, 0.5 M NaCl, 5% glycerol buffer, pH 7.5) and once with lysis buffer before bound protein was eluted stepwise using imidazole (50 to 250 mM). Purified MITF was visualized by SDS/PAGE and Coomassie staining, and protein-containing fractions

were pooled and dialyzed against buffers containing buffers decreasing concentrations of urea (25 mM Hepes, pH 7.5, 0.5 M NaCl, 5% glycerol, 4.0 to 0.0 M urea) at 4 °C. After dialysis, samples were flash frozen in aliquots in liquid nitrogen and stored at −80 °C before use.

To phosphorylate MITF in vitro, 2 μg of recombinant HIS-tagged MITF (1–100) was incubated 1 h at 37 °C with 100 ng of GSK3β (Abcam) and/or ERK2 (Sigma Aldrich) in the presence of cold ATP in a reaction diluted to 22 μL with kinase dilution buffer (5 mM Mops, pH 7.2, 5 mM $MgCl_2$, 0.4 mM EDTA, 1 mM EGTA, 2.5 mM glycerol 2-phosphate) before adding DTT to a final concentration of 0.25 mM. When both ERK and GSK3β were used, ERK2 was used first, and GSK3β was added after 30 min. Reactions were stopped by addition of 100 mM EDTA.

Proteomics Analysis. Proteins phosphorylated in vitro were subjected to chymotrypsin digest (Thermo Fisher) treatment according to the manufacturer's instructions, desalted using SepPak reversed phase columns, and injected into a liquid chromatography-tandem mass spectrometry (LC-MS/MS) platform (Dionex Ultimate 3000 nano LC and Q-Exactive HF). Sample separation was undertaken using a 50-cm-long EasySpray column (ES803; Thermo Fisher) with a 75-μm inner diameter and a gradient of 2 to 35% acetonitrile in 0.1% formic acid and 5% DMSO with a 250 nL/min flow rate for 60 min. MS1 spectra with a resolution of 60,000 and an ion target of 3 million were acquired for a maximum of 45 ms. MS/MS data were acquired after isolation with a mass window of 1.2 Th and fragmentation at 28% normalized collision energy (higher-energy collisional dissociation, resolution 30,000). PEAKS Server V.8.5 (Bioinformatics Solutions) and a Uniprot/Trembl database were used to analyze the LC-MS/MS data set to identify phosphorylation (S, T, Y), as well as oxidation (M) and deamidation (N, Q). Mass tolerance was 10 ppm for precursor and 0.5 Da for fragment mass, with a peptide level false discovery rate set to 1%. Freestyle 1.3 (Thermo Fisher) was used to generate extracted ion chromatograms of relevant peptides that were quantified after Gaussian smoothing (three data points).

MITF-CRM1 Interaction Assay. N-terminally GST-tagged CRM1 was expressed in *E. coli* after induction overnight at 18 °C with 0.5 mM isopropyl-β-D-thiogalactopyranoside (IPTG) and purified at 4 °C using glutathione beads from extracts of sonicated bacteria that had been precleared by centrifugation at 50,000 × *g* for 30 min at room temperature. Purified protein was released from the beads by cleavage using TEV protease. Recombinant CRM1 was then further purified using a MonoQ HP column and eluted using a 0 to 1 M NaCl gradient in a buffer containing 20 mM Tris (pH 7.5, 1 mM EGTA, 2 mM MgAc, 1 mM DTT, and 10% glycerol). Human HIS-tagged RAN protein was similarly expressed in *E. coli* but was purified by affinity chromatography on Ni-NTA beads. Bound RAN was eluted using 500 mM imidazole and subsequently purified using a Superdex-75 column (Amersham Biosciences) in 20 mM Tris (pH 8.0), 1 mM DTT, 10% (vol/vol) glycerol. To obtain a GTP-bound fraction, purified Ran was incubated with GTP at a 1,000-molar excess in 50 mM Hepes, pH 7.5, 10 mM EDTA, 4 mM DTT, 2 mM ATP at 30 °C for 30 min, before the reaction was halted using 15 mM $MgCl_2$ at 4 °C.

HIS-tagged amino acids 1 to 105 of the MITF-M isoform expressed in *E. coli* cells were expressed as described for RAN. After sonication in denaturing lysis buffer [50 mM Hepes, pH 7.5, 500 mM NaCl, 20 mM imidazole, 5% (vol/vol) glycerol, 10 mM β-mercaptoethanol, 6 M urea], MITF protein was isolated by direct binding to Ni-NTA beads. The beads were then washed extensively, and bound protein was refolded by stepwise decreasing the urea concentration from 6 M to 0 M using volumes of 10 mL and a 1 mL/min flow rate. Then, 100 pmol of MITF protein bound to Ni-NTA beads was used together with 50 pmol CRM1 with or without a twofold molar excess of GTP-bound Ran. Proteins were mixed in 400 μL binding buffer comprising 20 mM Hepes (pH 7.5), 2 mM magnesium acetate, 110 mM potassium acetate, 1 mM EGTA, 20 mM DTT, 0.005% Nonidet P-40, and 20 mM imidazole and rotated for 2 h at 4 °C. Beads were washed four times with binding buffer to remove unbound protein before addition of hot Laemmli buffer. Protein complexes were analyzed by SDS/PAGE, and CRM1 and RAN were detected by Western blotting.

Zebrafish. Two nanoliters of plasmid DNA containing the zebrafish *mitfa* gene promoter (62) driving WT and mutant fish MITF cDNA (25 ng/μL) together with Tol2 mRNA (35 ng/μL) was injected into *mitfa*-null *nacre* embryos at the one-cell stage and grown at 28.5 °C for 5 d. Embryos were then exposed briefly to white light to contract melanocytes and subsequently imaged before fixation in 4% PFA. The surface melanocytes in the head, trunk, and yolk sac were then counted. Quantitative analysis of melanocyte development in groups of fish injected with different mutant forms of MITF was carried out with the Minicab 16 statistical software (Minitab Inc). One-way ANOVA was used to determine the difference between two groups. For imaging expression of Mitfa, VC7 embryos (62) were grown for 24 h postinjection and processed for immunostaining using anti-FLAG antibody (F7425, rabbit 1:150; Sigma) and rabbit Alexa Fluor 488-conjugated secondary antibody (1:250) before visualization using a Leica confocal SP5 microscope at 10× magnification. For quantification of *mitfa* gene expression at 24 hours postfertilization by RT-PCR, *nacre* mutant fish have a point mutation C > T at position 337 in the Mitfa ORF, resulting in a premature TAA stop codon and truncated Mitfa protein. To distinguish transgenic *mitfa* from endogenous nacre *mitfa*, the last G nucleotide at the 3′ end of the reverse primer differs between WT and nacre so as not to amplify the mutant allele. The sequences of *mitfa* primers used for both RT-PCR and q-PCR are as follows: *mitfa*-F, 5′-CGCCGAGCACGGCATGACC-3′; and *mitfa*-WT-R, 5′-TGAAACTGGAATCGTGTTTGTCATTTG-3′. The size of product is 193 bp. Zebrafish β-actin was used as an internal control. The primer sequences for β-actin are as follows: actin-F, 5′-TGCCATGTATGTGGCCATCCA-3′; actin-R, 5′-ACCTCCAGACAGCACTGTGT-3′ with an amplicon of 602 bp; if there is genomic DNA contamination, an additional amplicon of 689 bp will be seen. For reproducibility, the Zebrafish experiments were repeated three times and were approved by the University of Edinburgh Animal Welfare and Ethical Review Body and undertaken in accordance with the *Animals (Scientific Procedures) Act* 1986. Zebrafish lines were bred, raised, and maintained as described (63).

Subcellular Fractionation. To separate out the cytosolic components of the cell from the nuclear fraction, trypsinized cells were lysed in cold Triton X lysis buffer (50 mM Tris-Cl, pH 7.5, 137.5 mM NaCl, 0.5% Triton X-100, 10% glycerol) supplemented with 1× Complete Protease Inhibitor and 1× PhosSTOP Phosphatase Inhibitor. The cell lysate was incubated on ice for 20 min and then centrifuged at 16,000 × *g* and 4 °C in a bench-top centrifuge for 15 min. The supernatant was the cytoplasmic fraction while the pellet was resuspended in 1× Laemmli sample buffer and taken to be the nuclear fraction. Both fractions were stored at −20 °C.

Luciferase Reporter Assay. Cells were plated overnight in 24-well plates (Corning) until 50% confluent and then transfected with two plasmids in a 1:1 ratio: a plasmid encoding *MITF* and a plasmid encoding the firefly luciferase gene under the control of the *TYR* promoter. Cells were harvested 48 h posttransfection by incubating with 100 μL of Passive Lysis Buffer (Promega) for 30 min at 4 °C on a rocking platform. Then, 20 μL of the lysate was mixed with 50 μL of Luciferase Assay Reagent (Promega) in a white 96-well plate (Corning), after which luminescence was detected with a GloMax-Multi Microplate Multimode Reader (Promega) luminometer.

ACKNOWLEDGMENTS. We thank Katherine Dowsett for assistance with the zebrafish experiments. Mass spectrometry analysis was performed in the Target Discovery Institute MS Laboratory led by Benedikt M. Kessler. This research was supported by the Agency for Science, Technology and Research Singapore (K.C.N.); Cancer Research UK (CRUK) Grant C38302/A12981, through a CRUK Oxford Centre Prize DPhil Studentship (to H.J.F.); The China Scholarship Council (L.L.); Wellcome Trust Career Development Fellowship 095751/Z/11/Z (to P.F. and S.P.); the Structural Genomics Consortium (S.K.); Arthritis Research UK Grant MP/19200 and Rosetrees Trust Grant M456 (to H.K.); The Research Fund of Iceland (E.S.); the Ludwig Institute for Cancer Research (C.R.G., S.A., and G.B.); the Kennedy Trust Fund (R.F.); The Medical Research Council Human Genetics Unit Programme MC_PC_U127585840 (to E.E.P. and Z.Z.); The European Research Council Grant ZF- MEL-CHEMBIO-g48489 (to E.E.P. and H.B.); and L'Oreal-Melanoma Research Alliance Grant 401181 (to E.E.P.). K.L.B.B. is supported by NIH Grants NIH 98571 and NIH 80728 and holds a Canada Research Chair (Tier 1).

1. Garraway LA, et al. (2005) Integrative genomic analyses identify MITF as a lineage survival oncogene amplified in malignant melanoma. *Nature* 436:117–122.
2. Lister JA, et al. (2014) A conditional zebrafish MITF mutation reveals MITF levels are critical for melanoma promotion vs. regression in vivo. *J Invest Dermatol* 134:133–140.
3. Hodgkinson CA, et al. (1993) Mutations at the mouse *microphthalmia* locus are associated with defects in a gene encoding a novel basic-helix-loop-helix-zipper protein. *Cell* 74:395–404.
4. Widlund HR, et al. (2002) Beta-catenin-induced melanoma growth requires the downstream target microphthalmia-associated transcription factor. *J Cell Biol* 158: 1079–1087.
5. Carreira S, et al. (2005) Mitf cooperates with Rb1 and activates p21Cip1 expression to regulate cell cycle progression. *Nature* 433:764–769.
6. Carreira S, et al. (2006) Mitf regulation of Dia1 controls melanoma proliferation and invasiveness. *Genes Dev* 20:3426–3439.

7. Cheli Y, et al. (2011) Mitf is the key molecular switch between mouse or human melanoma initiating cells and their differentiated progeny. *Oncogene* 30:2307–2318, and erratum (2011) 30:2390.
8. Hoek KS, et al. (2006) Metastatic potential of melanomas defined by specific gene expression profiles with no BRAF signature. *Pigment Cell Res* 19:290–302.
9. Hoek KS, Goding CR (2010) Cancer stem cells versus phenotype-switching in melanoma. *Pigment Cell Melanoma Res* 23:746–759.
10. Falletta P, et al. (2017) Translation reprogramming is an evolutionarily conserved driver of phenotypic plasticity and therapeutic resistance in melanoma. *Genes Dev* 31: 18–33.
11. Johannessen CM, et al. (2013) A melanocyte lineage program confers resistance to MAP kinase pathway inhibition. *Nature* 504:138–142.
12. Müller J, et al. (2014) Low MITF/AXL ratio predicts early resistance to multiple targeted drugs in melanoma. *Nat Commun* 5:5712.
13. Dugo M, et al. (2015) A melanoma subtype with intrinsic resistance to BRAF inhibition identified by receptor tyrosine kinases gene-driven classification. *Oncotarget* 6: 5118–5133.
14. Konieczkowski DJ, et al. (2014) A melanoma cell state distinction influences sensitivity to MAPK pathway inhibitors. *Cancer Discov* 4:816–827.
15. Giuliano S, et al. (2010) Microphthalmia-associated transcription factor controls the DNA damage response and a lineage-specific senescence program in melanomas. *Cancer Res* 70:3813–3822.
16. Zhang T, et al. (2015) Mitf is a master regulator of the v-ATPase, forming a control module for cellular homeostasis with v-ATPase and TORC1. *J Cell Sci* 128:2938–2950.
17. Ploper D, et al. (2015) MITF drives endolysosomal biogenesis and potentiates Wnt signaling in melanoma cells. *Proc Natl Acad Sci USA* 112:E420–E429.
18. Haq R, et al. (2013) Oncogenic BRAF regulates oxidative metabolism via PGC1α and MITF. *Cancer Cell* 23:302–315.
19. Vazquez F, et al. (2013) PGC1α expression defines a subset of human melanoma tumors with increased mitochondrial capacity and resistance to oxidative stress. *Cancer Cell* 23:287–301.
20. Bharti K, Liu W, Csermely T, Bertuzzi S, Arnheiter H (2008) Alternative promoter use in eye development: The complex role and regulation of the transcription factor MITF. *Development* 135:1169–1178.
21. Perera RM, et al. (2015) Transcriptional control of autophagy-lysosome function drives pancreatic cancer metabolism. *Nature* 524:361–365.
22. Miller AJ, Levy C, Davis IJ, Razin E, Fisher DE (2005) Sumoylation of MITF and its related family members TFE3 and TFEB. *J Biol Chem* 280:146–155.
23. Murakami H, Arnheiter H (2005) Sumoylation modulates transcriptional activity of MITF in a promoter-specific manner. *Pigment Cell Res* 18:265–277.
24. Bertolotto C, et al.; French Familial Melanoma Study Group (2011) A SUMOylation-defective MITF germline mutation predisposes to melanoma and renal carcinoma. *Nature* 480:94–98.
25. Yokoyama S, et al. (2011) A novel recurrent mutation in MITF predisposes to familial and sporadic melanoma. *Nature* 480:99–103.
26. Price ER, et al. (1998) Lineage-specific signaling in melanocytes. C-kit stimulation recruits p300/CBP to microphthalmia. *J Biol Chem* 273:17983–17986.
27. Wu M, et al. (2000) c-Kit triggers dual phosphorylations, which couple activation and degradation of the essential melanocyte factor Mi. *Genes Dev* 14:301–312.
28. Xu W, et al. (2000) Regulation of microphthalmia-associated transcription factor MITF protein levels by association with the ubiquitin-conjugating enzyme hUBC9. *Exp Cell Res* 255:135–143.
29. Mansky KC, Sankar U, Han J, Ostrowski MC (2002) Microphthalmia transcription factor is a target of the p38 MAPK pathway in response to receptor activator of NF-kappa B ligand signaling. *J Biol Chem* 277:11077–11083.
30. Bronisz A, et al. (2006) Microphthalmia-associated transcription factor interactions with 14-3-3 modulate differentiation of committed myeloid precursors. *Mol Biol Cell* 17:3897–3906.
31. Martina JA, Puertollano R (2013) Rag GTPases mediate amino acid-dependent recruitment of TFEB and MITF to lysosomes. *J Cell Biol* 200:475–491.
32. Takeda K, et al. (2000) Ser298 of MITF, a mutation site in Waardenburg syndrome type 2, is a phosphorylation site with functional significance. *Hum Mol Genet* 9: 125–132.
33. Drewry DH, Willson TM, Zuercher WJ (2014) Seeding collaborations to advance kinase science with the GSK Published Kinase Inhibitor Set (PKIS). *Curr Top Med Chem* 14: 340–342.
34. Meijer L, et al. (2003) GSK-3-selective inhibitors derived from Tyrian purple indirubins. *Chem Biol* 10:1255–1266.
35. Bennett DC (2016) Genetics of melanoma progression: The rise and fall of cell senescence. *Pigment Cell Melanoma Res* 29:122–140.
36. Fedorenko IV, Gibney GT, Sondak VK, Smalley KS (2015) Beyond BRAF: Where next for melanoma therapy? *Br J Cancer* 112:217–226.
37. Vredeveld LC, et al. (2012) Abrogation of BRAFV600E-induced senescence by PI3K pathway activation contributes to melanomagenesis. *Genes Dev* 26:1055–1069.
38. Delmas V, et al. (2007) Beta-catenin induces immortalization of melanocytes by suppressing p16INK4a expression and cooperates with N-Ras in melanoma development. *Genes Dev* 21:2923–2935.
39. Hemesath TJ, Price ER, Takemoto C, Badalian T, Fisher DE (1998) MAP kinase links the transcription factor microphthalmia to c-Kit signalling in melanocytes. *Nature* 391: 298–301.
40. Frame S, Cohen P (2001) GSK3 takes centre stage more than 20 years after its discovery. *Biochem J* 359:1–16.
41. Bensimon A, et al. (2010) ATM-dependent and -independent dynamics of the nuclear phosphoproteome after DNA damage. *Sci Signal* 3:rs3.
42. Takebayashi K, et al. (1996) The recessive phenotype displayed by a dominant negative microphthalmia-associated transcription factor mutant is a result of impaired nucleation potential. *Mol Cell Biol* 16:1203–1211.
43. Kutay U, Güttinger S (2005) Leucine-rich nuclear-export signals: Born to be weak. *Trends Cell Biol* 15:121–124.
44. Fornerod M, Ohno M, Yoshida M, Mattaj IW (1997) CRM1 is an export receptor for leucine-rich nuclear export signals. *Cell* 90:1051–1060.
45. Kırlı K, et al. (2015) A deep proteomics perspective on CRM1-mediated nuclear export and nucleocytoplasmic partitioning. *eLife* 4:e11466.
46. Weis K (2003) Regulating access to the genome: Nucleocytoplasmic transport throughout the cell cycle. *Cell* 112:441–451.
47. Kalderon D, Roberts BL, Richardson WD, Smith AE (1984) A short amino acid sequence able to specify nuclear location. *Cell* 39:499–509.
48. Wen W, Meinkoth JL, Tsien RY, Taylor SS (1995) Identification of a signal for rapid export of proteins from the nucleus. *Cell* 82:463–473.
49. Takeda K, et al. (2002) Mitf-D, a newly identified isoform, expressed in the retinal pigment epithelium and monocyte-lineage cells affected by Mitf mutations. *Biochim Biophys Acta* 1574:15–23.
50. Kaffman A, Rank NM, O'Neill EM, Huang LS, O'Shea EK (1998) The receptor Msn5 exports the phosphorylated transcription factor Pho4 out of the nucleus. *Nature* 396:482–486.
51. Alt JR, Cleveland JL, Hannink M, Diehl JA (2000) Phosphorylation-dependent regulation of cyclin D1 nuclear export and cyclin D1-dependent cellular transformation. *Genes Dev* 14:3102–3114.
52. Marsh Durban V, Deuker MM, Bosenberg MW, Phillips W, McMahon M (2013) Differential AKT dependency displayed by mouse models of $BRAF^{V600E}$-initiated melanoma. *J Clin Invest* 123:5104–5118.
53. Nogueira C, et al. (2010) Cooperative interactions of PTEN deficiency and RAS activation in melanoma metastasis. *Oncogene* 29:6222–6232.
54. Dankort D, et al. (2009) Braf(V600E) cooperates with Pten loss to induce metastatic melanoma. *Nat Genet* 41:544–552.
55. Stambolic V, Woodgett JR (1994) Mitogen inactivation of glycogen synthase kinase-3 beta in intact cells via serine 9 phosphorylation. *Biochem J* 303:701–704.
56. Takeda K, et al. (2000) Induction of melanocyte-specific microphthalmia-associated transcription factor by Wnt-3a. *J Biol Chem* 275:14013–14016.
57. Dorsky RI, Raible DW, Moon RT (2000) Direct regulation of *nacre*, a zebrafish MITF homolog required for pigment cell formation, by the Wnt pathway. *Genes Dev* 14:158–162.
58. Rabbani P, et al. (2011) Coordinated activation of Wnt in epithelial and melanocyte stem cells initiates pigmented hair regeneration. *Cell* 145:941–955.
59. Habib SJ, et al. (2013) A localized Wnt signal orients asymmetric stem cell division in vitro. *Science* 339:1445–1448.
60. Pogenberg V, et al. (2012) Restricted leucine zipper dimerization and specificity of DNA recognition of the melanocyte master regulator MITF. *Genes Dev* 26:2647–2658.
61. Grill C, et al. (2013) MITF mutations associated with pigment deficiency syndromes and melanoma have different effects on protein function. *Hum Mol Genet* 22: 4357–4367.
62. Zeng Z, Johnson SL, Lister JA, Patton EE (2015) Temperature-sensitive splicing of mitfa by an intron mutation in zebrafish. *Pigment Cell Melanoma Res* 28:229–232.
63. Westerfield M (2000) *The Zebrafish Book: A Guide for the Laboratory Use of Zebrafish (Danio rerio)* (Univ Oregon Press, Eugene, OR), 4th Ed.